



HAL
open science

Northward drift of the Azores plume in the Earth's mantle

Maëlis Arnould, Jérôme Ganne, Nicolas Coltice, Xiaojun Feng

► **To cite this version:**

Maëlis Arnould, Jérôme Ganne, Nicolas Coltice, Xiaojun Feng. Northward drift of the Azores plume in the Earth's mantle. *Nature Communications*, 2019, 10, pp.3235. 10.1038/s41467-019-11127-7 . hal-03228578

HAL Id: hal-03228578

<https://hal.science/hal-03228578>

Submitted on 18 May 2021

HAL is a multi-disciplinary open access archive for the deposit and dissemination of scientific research documents, whether they are published or not. The documents may come from teaching and research institutions in France or abroad, or from public or private research centers.

L'archive ouverte pluridisciplinaire **HAL**, est destinée au dépôt et à la diffusion de documents scientifiques de niveau recherche, publiés ou non, émanant des établissements d'enseignement et de recherche français ou étrangers, des laboratoires publics ou privés.

1 Northward drift of the Azores plume in the Earth's mantle

2 Maëlis Arnould^{1,2}, Jérôme Ganne³, Nicolas Coltice⁴, Xiaojun Feng⁵

3
4
5 1 - LGL TPE, UMR CNRS 5276 (CNRS, ENS, Université Lyon1), Ecole Normale Supérieure de Lyon 69364
6 Lyon cedex 07, France

7 2 – EarthByte Group, School of Geosciences, Madsen Building F09, University of Sydney, NSW, 2006,
8 Australia

9 3 - IRD, CNRS, GET, Université Toulouse III, 14 Avenue Edouard Belin, 31400 Toulouse, France

10 4 - Laboratoire de Géologie, École Normale Supérieure, CNRS UMR 8538, PSL Research University, Paris
11 75005, France

12 5 - School of Safety Engineering, China University of Mining and Technology, Jiangsu, China

13 14 15 16 17 18 **ABSTRACT**

19
20 The fixity of mantle plumes has been a cornerstone assumption for the reconstruction of tectonic plate motions¹.
21 However, paleomagnetic records and age progression along hotspot tracks have suggested substantial drift of
22 plumes below the Pacific plate². Identifying the individual motion of a plume usually requires a long and
23 continuous chain of seamounts, and precise geochronological and paleomagnetic data. Hence Hawaii is the only
24 plume with clear evidence of drift so far^{3,4}. Here, we use plume-derived basalts from the Mid-Atlantic ridge
25 (MAR) to map the mantle temperature over a large region in the upper mantle centered on the Azores. We show
26 the thermal anomaly associated with the plume is asymmetric, spreading over ~2,000 km southwards and ~1,000
27 km northwards. The extent, shape and asymmetry of this anomaly cannot be accounted by a stationary plume.
28 Using a 3D spherical mantle convection model allowing for self-consistent plate-like tectonics and drifting
29 plumes, we show that the Azores plume moved northwards by 1-2 cm/yr from 85 Ma, independently from other
30 Atlantic plumes, developing the Great-Meteor and Corner Rise volcanic chains.

31 The Azores plateau is an oceanic area of about 135,000 km², with a magmatic center located about 100-200 km^{5,6}
32 away from the MAR axis. The spatial correlation between bathymetric highs^{6,7}, anomalously thick crust^{8,9},
33 gravity anomalies¹⁰ and geochemical signatures¹¹ along the MAR point to an interaction between the ridge and a
34 deep mantle plume. Both upper-mantle¹²⁻¹⁴ and global seismic tomography studies¹⁵ describe the presence of a
35 narrow and rather vertical low seismic velocity conduit beneath the Azores. This seismic anomaly extends in the
36 lower mantle¹⁵ and the high ⁴He/³He ratios of the lavas¹⁶ further consolidates the deep origin of the Azores
37 plume.

38

39 The symptoms of the plume-ridge interaction spread over a large region. The bathymetric high along the ridge
40 forms a bulge declining by 2.5 km over 1000 km towards the North, and by 2 km over 3000 km towards the
41 South^{6,7} (**Fig. 1 SI**). High resolution tomographic models of the upper mantle support the presence of an
42 asymmetric slow velocity region spreading along the ridge over 3,000 km (see **Fig. 1**). These observations
43 suggest an asymmetric thermal anomaly along the MAR, elongated southwards. To characterize the temperature
44 of the mantle over that region, we have analyzed the composition of mid-oceanic ridge basalts (MORBs).

45

46 MORBs are extracted from a partially melted region in the shallow ambient convective mantle. Their chemistry
47 likely reflects the potential temperature (T_p) of this region, corresponding to the temperature that the ambient
48 mantle would reach, should it raise adiabatically to the Earth surface without melting¹⁷. Global systematics of the
49 chemistry of MORBs suggest T_p variations of 200° to 250°C along, and immediately below, mid-oceanic
50 ridges^{8,13}, challenging some previous estimates (~100°C^{18,19}). However, whether or not these variations simply
51 reflect chemical heterogeneities in the mantle source, inappropriate corrections for fractionation²⁰ or the presence
52 of fluids in the magmatic source²¹ remains a source of debate.

53

54 A more selective but secure approach relies on the chemical composition of primary magma formed by melting
55 of dry, fertile peridotite, with limited fractional crystallization prior to magma emplacement in the crust.
56 Inferences, though limited, already suggest that MORBs appear often too differentiated to yield T_p estimates
57 with the PRIMELT method^{22,23}. Conversely, intraplate volcanism, which also gives birth to primary magmas
58 through decompression melting of deeper and hotter sections of the mantle (e.g. mantle plume), can provide
59 successful solutions of calculation with PRIMELT (less than 10%).

60

61 Here, we propose to integrate this set of PRIMELT values when discussing the significance of T_p variations
62 along the MAR close to the Azores, acknowledging that interactions through time between the Azores plume and
63 the ridge produce a wide range of T_p estimates. Geochemical data considered in this study come from Gale et al.,
64 2013²⁴ who compiled an extensive chemical database of near zero-age (i.e. < ca. 300 kyrs) MORBs collected
65 along the axis of mid-oceanic ridges (**Fig. 2 SI to 7 SI**). We focus on the northern sections of the MAR (**Fig. 2**),
66 from latitude 0 to 90°N where data is the most abundant. **Fig. 3b** illustrates the distribution of T_p obtained with
67 PRIMELT along the MAR, showing a peak in temperature centered on Iceland (1530°C) and Azores (1520°C),
68 with decreasing mean temperatures toward the north and the south of the volcanic archipelago. At a smaller
69 scale, an apparent asymmetric zoning is observed around Azores (> 2,000 km): temperature decreases by 60°C

70 over ~2,000 km (0.03°C/km) towards the south while it decreases by 60°C over at least 500 km (0.12°C/km)
71 towards the north.

72

73 **Fig. 2** and **3** show that the decrease in temperature correlates with a chemical depletion in calcium for MORBs.
74 Calcium depletion is related to (i) an increasing melting of pyroxenite in the mantle, given the lower solidus of
75 pyroxenites relative to peridotites; or (ii) an increasing fractionation (crystallization then subtraction) of
76 magmatic pyroxenes during the ascent of primary melts through the lithospheric column, with such
77 crystallization being primarily controlled by the temperature of the mantle or the crustal section crossed by these
78 melts. In both cases, the depletion in calcium for MORBs is indicative of a colder oceanic lithosphere or
79 asthenospheric mantle below the MAR. Petrological equilibrium curves²⁵ show that MORBs sampled away from
80 Iceland and Azores crystallized pyroxenes at greater pressures and that the decrease in pressure correlates with
81 the distance to hotspots in both cases (**Fig. 3a**). This supports the idea of mantle temperature control on calcium
82 depletion in MORBs, and suggests that beneath Iceland or Azores, pyroxenes crystallize only in the oceanic
83 crust while further away, pyroxenes mostly crystallize in the mantle section.

84

85 Theoretical studies of plume-ridge interactions^{26–28} have characterized relationships between extent of hot plume
86 material spreading along the ridge (called waist) and its volume flux. The estimates for the volume flux vary
87 between 51 m³/s, based on the spreading rate of the MAR²⁹ to 90 m³/s, deduced from the topographic swell
88 around the hotspot³⁰. Accounting for a waist > 2,000 km consistent with bathymetry⁶, seismic tomography (**Fig.**
89 **1**) and our temperature estimates, drives the theoretical models to unrealistic volume flux predictions, being
90 close to 400 m³/s³¹. Neither can the presence of anomalously high temperatures more than 2,000 km south of the
91 plume be accounted for by a burst of plume activity in the past. Such increase in the volume flux or temperature
92 of the plume was proposed for the Azores about 10 My ago based on V-shaped gravity and topographic
93 structures recognized south of the Azores³², but would have led to a discontinuous gradient of temperature
94 decrease with a local increase of T_p of about 70°C, at about 600 km from the hotspot location and lasting only a
95 few million years²⁸.

96

97 We explore the hypothesis that the thermal anomaly below the MAR corresponds to the thermal wake behind the
98 Azores plume, formed by a relative motion between the African plate and the plume³³. The southward shearing
99 of the hot mantle flux would be a consequence of the northward motion of the Azores conduit relative to other
100 Atlantic plumes. Both the hotspot chains of St-Helena and Tristan show that the African plate is moving towards
101 the east-north-east relative to their source³⁴ (**Fig. 8 SI**). This motion of the African plate is consistent with
102 absolute kinematics deduced from anisotropy in the uppermost mantle³⁵. The scenario of a northward motion of
103 the Azores plume relative to the African plate also supports the proposal that the Corner Rise and the Great
104 Meteor oceanic plateaus are the hotspot chains of the Azores built over the past 85 My³⁶. To further evaluate the
105 hypothesis of a moving plume leaving such an elongated asymmetric thermal wake below the ridge, we compute
106 a 3D spherical convection model in which self-consistent plate tectonics interact with naturally drifting plumes
107 (see **Methods**). Instead of using multiple regional models and imposing potentially unphysical constraints to our
108 system to generate relative motions below a ridge, we compute one global model with multiple plumes where a
109 situation like the MAR-Azores interaction naturally emerges from the self-organizing system.

110

111 The numerical model produces surface velocities, heat flow and plate size distributions comparable to Earth. We
112 detect about 25 plumes on average at each time step. These plumes have a $210\pm 45^\circ\text{C}$ average temperature excess
113 with respect to the ambient mantle, an upper mantle vertical velocity of 25.6 ± 8.3 cm/yr, conduit diameters of
114 200 ± 150 km, and volume fluxes of 25 ± 15 m³/s. We identify a total of 76 distinct plumes over the 320 My of
115 model duration, moving laterally relative to a no-net rotation surface at 1.75 ± 0.38 cm/yr. Relative motions
116 between hotspots are limited to 1.2 ± 0.4 cm/yr. We observe that 46 of them interact at some point with ridges,
117 either ponding below them or contributing to their propagation. We identified one plume with a volume flux of
118 45 ± 5 m³/s moving along a stable ridge (ridge axis 1) at about 1 cm/yr over 70 My before escaping it at a lateral
119 velocity reaching 2.9 cm/yr (**Fig. 4, Table 2 SI**).

120

121 **Fig. 4** shows the temporal evolution of the potential temperature at 110 km depth along ridge axes 1 (**Fig. 4e-h**)
122 and 2 (**Fig. 4i-l**). At this depth, the average temperature below the thermal boundary layer is about 1,300°C. In
123 **Fig. 4a-d**, the thermal anomaly extends along ridge axis 1 from more than 3,500 km at 10 My to 2,000 km at 100
124 My, as the plume moves away from the ridge system. A thermal gradient asymmetry along ridge axis 1 is
125 persistent throughout the sequence, even when the plume is 1,000 km away from the ridge (**Fig. 4d,h,l**). The
126 horizontal temperature gradient is sharp southeastwards in the direction of plume motion, reaching up to
127 1°C/km, while it is 0.05°C/km northwestwards. Ridge axis 2 is near perpendicular to the plume motion between
128 10 and 40 My. Throughout that period, the potential temperature profile is symmetric as expected (**Fig. 4e**).
129 From 70 My, the temperature profile becomes asymmetric, being sharper northwestwards (thermal gradient of
130 0.8°C/km), as the plume now moves at a small angle relative to ridge axis 2. This asymmetry compares to
131 observations at the MAR in the vicinity of the Azores hotspot (about 0.8°C/km towards the North and
132 0.03°C/km towards the South according to **Fig. 3b**). Therefore, we propose that an absolute northward motion of
133 the Azores plume at a rate of about 1-2 cm/yr explains both the extent and asymmetry of the observed thermal
134 anomaly, as shown on **Fig. 4**. The proposed role of the Azores plume in the building of Corner Rise and Great
135 Meteor plateaus (located about 1,000 km away from the present-day location of the plume) from 85 My to 20
136 My^{36,37} is consistent with velocities of the order of 1-2 cm/yr. Moreover, such velocities fit with the proposed
137 migration velocity of the Azores plume away from the MAR at 10 ± 5 My³⁶.

138

139 Our study shows that characterizing thermal anomalies linked with plume-ridge interactions has the potential to
140 unravel absolute plume motions, questioning our knowledge of mantle plumes. Hence, the motion of the Azores
141 plume we described here appears at odds with the common view that Atlantic plumes are stable³⁸⁻⁴⁰, which is
142 mainly based on St-Helena and Tristan da Cunha/Gough hotspot tracks. However, the proposed motion of the
143 Azores plume is consistent with evidences of moving mantle plumes⁴¹. Tarduno et al., 2003⁴ proposed that the
144 plume beneath Hawaii could have moved southward by > 4 cm/yr between 81 and 47 Ma. Moreover, in a fully-
145 dynamic convective system, plume conduits are likely to be swept away by moving slabs in the lower mantle at
146 rates exceeding 5 cm/yr⁴², or by the ambient mantle flow⁴³. The possible anchorage of the Azores plume on the
147 edge of a dense and stable large low shear velocity province (LLSVP), as suggested in tomographic models⁴⁴, is
148 not accounted by our convection model. However, convection calculations do not show enhanced fixity of
149 plumes with chemical anomalies at the core-mantle boundary⁴⁵. Also, slow deformation of the edges of LLSVPs

150 produce plume motions of the order of 1 cm/yr⁴⁶, and plumes can propagate longitudinally along the edges of
151 LLSVPs which undergo significant thermomechanical or thermochemical instabilities⁴⁷.

152 **METHOD**

153 **PRIMELT**

154 Mantle T_p calculation using *PRIMELT* is based on the MgO content of the primary magma, and MgO typically
155 correlates with FeO. The calculations require that FeO be obtained from FeO_T (total iron reported as a single
156 oxide) and this can be estimated assuming $Fe_2O_3/TiO_2 = 0.5$ or assuming a constant redox condition in the
157 magmatic source ($Fe_{2+}/\Sigma Fe = 0.9$ or 0.8). We tested different hypotheses and results are given in **Fig. 2 SI**.
158 Uncertainties that arise by calculating FeO using $Fe_2O_3/TiO_2=0.5$ instead of $FeO/FeO_T = 0.9$ propagate to
159 uncertainties in mantle T_p lower than 30 °C for high-Ti type lavas ($TiO_2 > 1$ wt%) up to 60 °C for low-Ti types
160 ($TiO_2 < 0.5$ wt%). MORBs are dominantly characterized by Ti content > 1 wt% (**Fig. 2d SI**). As such, alternative
161 adoption of a Ti-dependent redox condition is unlikely to affect our calculation toward more elevated T_p .
162 Consistently, a more oxidizing ratio of $Fe_{2+}/\Sigma Fe = 0.8$ will decrease FeO in the primary magma, yielding lower
163 MgO and lower mantle T_p but such general decrease will not change our general conclusions because it involves
164 the whole set of data.

165

166 The petrological software is calibrated by anhydrous melting experiments on fertile peridotite, and its application
167 to lavas assumes a similar fertile and dry peridotite source. Uncertainties in fertile peridotite composition do not
168 lead to significant errors in mantle T_p ⁴⁸. Conversely, melting of wet peridotite is likely to result in MgO values
169 that are too elevated. We excluded all samples that have undergone augite and/or plagioclase fractionation as
170 indicated by depletion of CaO and Al_2O_3 or enrichment in FeO. Such discrepancies can be highlighted in a
171 simple graph by plotting the chemistry of sample against its “liquid line of descent” (i.e. LLD, **Fig. 3 SI**). Our
172 calculations have been filtered according to a graphic procedure⁴⁸ leading to reduced uncertainties that arise from
173 pyroxenite source lithology, source volatile content from metasomatized peridotite, and clinopyroxene
174 fractionation (**Fig. 4 SI**). We assume that the remaining samples have been affected only by minor amounts of
175 olivine addition and subtraction. Solutions of our calculation are provided in the supplementary material (**Table**
176 **1 SI**).

177

178 **Fig. 2** and **3** unravels the chemical changes of MORBs along the MAR. The database records slightly elevated
179 CaO (wt%) values for MORBs centered on Azores (~40° N) and a progressive decrease further south and north
180 of the archipelagos, following a bell-shaped evolution. The percentage of samples for which PRIMELT predicts
181 a primary magma composition depleted in calcium, by comparison with primary magmas deriving from
182 peridotite-source, is given in **Fig. 2b**. Ca-depletion is minimal in the Azores region. It progressively increases in
183 the south and north of the archipelagos, raising its maximum values (~100%) along the Gakkel ridge that is
184 positioned on the northern segments of the MAR (**Fig. 5 SI**). Such differences in calcium cannot solely be
185 explained by a fractionation of olivine (forsterite : Mg-rich endmember) and either require an increasingly
186 subtraction of pyroxene (diopside : Mg_Ca-rich endmember) from the primary magma and/or an increasingly
187 melting of Ca-depleted source (pyroxenites) in the mantle⁴⁸ which, we infer, must be related to changes in the
188 mantle temperature below the MAR.

189

190 A cooler mantle will promote pyroxenite melting over peridotite because of its lower temperature. Likewise, low
191 thermal gradients in a mantellic section will promote the crystallization and sequestration of pyroxene at deeper

192 levels, decreasing the content of Ca in the residual melt. Elevated T_p values ($> 1500^\circ\text{C}$) are observed in the north
193 of the Azores archipelagos, extending to Iceland. A progressive decrease in temperature is observed southwards
194 of the Azores and a marked decrease northwards of the Azores, giving the appearance of asymmetric thermal
195 structure. However, a gap of data exists between 45° and 55° of north latitude (**Fig. 6** and **7 SI**). This section is
196 associated with a change in the orientation of the ridge, which here operates with a strong strike-slip component
197 (e.g. Charlie Gibbs's fault). The depth of pyroxene fractionation for MORBs was estimated using the equation
198 (6) of ²⁵ and results are given in **Fig. 3a**. MORBs in which olivine and plagioclase fractionation likely occurred
199 have been filtered out as discussed in Herzberg, 2004 ²⁵, these have $\text{CaO} > -0.3*\text{MgO} + 14.5$. As expected, lower
200 pressures of crystallization are observed around Azores and Iceland where elevated T_p have been calculated. The
201 pressures of crystallization increase with decreasing T_p , as observed in the south of Azores. The highest
202 pressures are observed for MORBs associated with ridge segment terminations (e.g. Gakkel ridge).

203

204 NUMERICAL MODELING

205

206 We use the thermochemical convection code StagYY⁴⁹ to model mantle convection in 3D spherical geometry
207 with continental lithospheric rafts and self-generation of plate-like tectonics at its surface. We solve the
208 equations of mass, momentum and energy conservation under the Boussinesq approximation. The Rayleigh
209 number of the system, based on the temperature drop across the layer is 10^7 , which results in a convective vigor
210 comparable to the Earth. All mantle parameters are constant with depth, except the thermal expansivity
211 coefficient (decreasing by a factor of 3 throughout the mantle), and the viscosity, which varies with temperature
212 T and pressure P as in Coltice and Shephard, 2018⁵⁰. The activation energy is 146 kJ/mol, implying 7 orders of
213 viscosity variations. The activation volume is $13.8 \text{ cm}^3/\text{mol}$, and we impose a viscosity jump by a factor of 30 at
214 660 km, consistently with postglacial rebound and geoid modeling^{51,52}.

215 We introduce pseudo-plasticity⁵³ to generate plate-like behaviour (plate boundaries emerge, they are not
216 imposed). After exploration of the parameter space, we choose a yield stress value of 48 MPa for the oceanic
217 lithosphere, so that the dynamic regime produces a plate-like behavior. The surface yield stress is 10 and 20
218 times higher for the margins and the interior of continental rafts respectively, to avoid their excessive mechanical
219 erosion. The yield stress varies with depth by a factor of 1.8 MPa/km for all materials.

220 We first run the model to reach a thermal statistical steady state. Then, we compute a total evolution of 400 My.
221 Such model is at the limit of computation capabilities and required about 7 weeks of computing time on a
222 parallel supercomputer of the National Computational Infrastructure (Australia). In the numerical solution,
223 mantle plumes originate from the CMB where the heat flow is about 5 TW. Internal heat is produced at a rate of
224 about $8.5 \cdot 10^{-12} \text{ W/kg}$. Surface heat flow reaches 34 TW, and the root-mean square surface velocity is 3.26
225 cm/yr. Plumes and plate boundaries are emergent structures, not imposed in such models. All plumes can
226 spontaneously move relatively to a no-net rotating surface. After the run, we examine these structures produced
227 in a self-consistent manner by the system of equations.

228 REFERENCES

229

- 230 1. Morgan, J. P. Deep mantle convection plumes and plate motions. *Am. Assoc. Pet. Geol. Bull.* **56**, 203–
231 213 (1972).
- 232 2. Torsvik, T. H., Voo, R. Van Der & Red, T. F. Relative hotspot motions versus True Polar Wander. *Earth*
233 *Planet. Sci. Lett.* **202**, (2002).
- 234 3. Konrad, K. *et al.* On the relative motions of long-lived Pacific mantle plumes. *Nat. Commun.* (2018).
235 doi:10.1038/s41467-018-03277-x
- 236 4. Tarduno, J. A. *et al.* The Emperor Seamounts : Southward Motion of the Hawaiian Hotspot Plume in
237 Earth’s Mantle. *Science.* **301**, 1064–1070 (2003).
- 238 5. Schilling, J.-G. Fluxes and excess temperatures of mantle plumes inferred from their interaction with
239 migrating mid-oceanic ridges. *Nature* **352**, 397–403 (1991).
- 240 6. Ito, G. & Lin, J. Oceanic spreading center– hotspot interactions: Constraints from along-isochron
241 bathymetric and gravity anomalies. *Geology* 657–660 (1995).
- 242 7. Vogt, P. R. Plumes, subaxial pipe flow, and topography. *Earth Planet. Sci. Lett.* **29**, 309–325 (1976).
- 243 8. Klein, E. M. & Langmuir, C. H. Global correlations of ocean ridge basalt chemistry with axial depth and
244 crustal thickness. *J. Geophys. Res.* **92**, 8089–8115 (1987).
- 245 9. Wang, T., Lin, J., Tucholke, B. & Chen, Y. J. Crustal thickness anomalies in the North Atlantic Ocean
246 basin from gravity analysis. *Geochemistry, Geophys. Geosystems* **12**, (2011).
- 247 10. Thibaud, R., Gente, P. & Maia, M. A systematic analysis of the Mid-Atlantic Ridge morphology and
248 gravity between 15°N and 40°N: constraints on the thermal structure. *J. Geophys. Res.* **103**, 24,223–
249 24,243 (1998).
- 250 11. Dosso, L., Bougault, H., Langmuir, C., Bollinger, C. & Bonnier, O. The age and distribution of mantle
251 heterogeneity along the Mid-Atlantic Ridge (31 – 41°N). *Earth Planet. Sci. Lett.* **170**, 269–286 (1999).
- 252 12. Silveira, G. *et al.* Azores hotspot signature in the upper mantle. *J. Volcanol. Geotherm. Res.* **156**, 23–34
253 (2006).
- 254 13. Dalton, C. A., Langmuir, C. H. & Gale, A. Geophysical and Geochemical Evidence for Deep
255 Temperature Variations Beneath Mid-Ocean Ridges. *Science.* **344**, (2014).
- 256 14. Pilidou, S., Priestley, K. & Debayle, E. Rayleigh wave tomography in the North Atlantic : high
257 resolution images of the Iceland, Azores and Eifel mantle plumes. *Lithos* **79**, 453–474 (2005).
- 258 15. French, S. W. & Romanowicz, B. Broad plumes rooted at the base of the Earth’s mantle beneath major
259 hotspots. *Nature* **525**, 95–99 (2015).
- 260 16. Moreira, M., Doucelance, R., Kurz, M. D., Dupré, B. & Allègre, C. J. Helium and lead isotope
261 geochemistry of the Azores Archipelago. *Earth Planet. Sci. Lett.* **169**, 189–205 (1999).
- 262 17. McKenzie, D. & Bickle, M. J. The Volume and Composition of Melt Generated by Extension of the
263 Lithosphere. *J. Petrol.* **29**, (1988).
- 264 18. Shen, Y. & Forsyth, D. W. Geochemical constraints on initial and final depths of melting beneath mid-
265 ocean ridge. *J. Geophys. Res.* (1995). doi:10.1029/94JB02768
- 266 19. Presnall, D. C., Urdinsson, G. U. H. G. & Walter, M. J. Generation of mid-ocean ridge basalts at
267 pressures from 1 to 7 GPa. *Geochim. Cosmochim. Acta* **66**, 2073–2090 (2002).

- 268 20. Niu, Y. & O'Hara, M. J. Global Correlations of Ocean Ridge Basalt Chemistry with Axial Depth : a
269 New Perspective. *J. Petrol.* **49**, (2008).
- 270 21. Cottrell, E. & Kelley, K. A. Redox heterogeneity in MORB as a function of mantle source. *Science.* **340**,
271 1314–1317 (2013).
- 272 22. Herzberg, C. *et al.* Temperatures in ambient mantle and plumes: Constraints from basalts, picrites, and
273 komatiites. *Geochemistry Geophys. Geosystems* **8**, (2007).
- 274 23. Ganne, J. & Feng, X. Magmatism : A crustal and geodynamic perspective. *J. Struct. Geol.* (2018).
275 doi:10.1016/j.jsg.2018.02.002
- 276 24. Gale, A., Dalton, C. A., Langmuir, C. H., Su, Y. & Schilling, J.-G. The mean composition of ocean ridge
277 basalts. *Geochemistry Geophys. Geosystems* **14**, (2013).
- 278 25. Herzberg, C. Partial Crystallization of Mid-Ocean Ridge Basalts in the Crust and Mantle. *J. Petrol.* **45**,
279 2389–2405 (2004).
- 280 26. Ribe, N. M., Christensen, U. R. & Theiging, J. The dynamics of plume-ridge interaction , 1 : Ridge-
281 centered plumes. **134**, 155–168 (1995).
- 282 27. Ito, G., Shen, Y., Hirth, G. & Wolfe, C. J. Mantle flow, melting, and dehydration of the Iceland mantle
283 plume. *Earth Planet. Sci. Lett.* **165**, 81–96 (1999).
- 284 28. Albers, M. & Christensen, U. R. Channeling of plume flow beneath mid-ocean ridges. *Earth Planet. Sci.*
285 *Lett.* **187**, 207–220 (2001).
- 286 29. Sleep, N. H. Hotspots and Mantle Plumes: Some Phenomenology. *J. Geophys. Res.* **95**, 6715–6736
287 (1990).
- 288 30. Crosby, A. G. & Mckenzie, D. An analysis of young ocean depth , gravity and global residual
289 topography. *Geophys. J. Int.* **178**, 1198–1219 (2009).
- 290 31. Ito, G., Lin, J. & Graham, D. Observational and theoretical studies of the dynamics of mantle plume-mid
291 ocean ridge interaction. *Rev. Geophys.* **41**, 1017 (2003).
- 292 32. Cannat, M. *et al.* Mid-Atlantic Ridge – Azores hotspot interactions : along-axis migration of a hotspot-
293 derived event of enhanced magmatism 10 to 4 Ma ago. *Earth Planet. Sci. Lett.* **173**, 257–269 (1999).
- 294 33. Moore, W. B., Schubert, G. & Tackley, P. Three-Dimensional Simulations of Plume-Lithosphere
295 Interaction at the Hawaiian Swell. *Science.* **279**, 1008–1012 (1998).
- 296 34. Torsvik, T. H., Steinberger, B., Gurnis, M. & Gaina, C. Plate tectonics and net lithosphere rotation over
297 the past 150 My. *Earth Planet. Sci. Lett.* **291**, 106–112 (2010).
- 298 35. Kreemer, C. Absolute plate motions constrained by shear wave splitting orientations with implications
299 for hot spot motions and mantle flow. *J. Geophys. Res.* **114**, 1–18 (2009).
- 300 36. Gente, P., Maia, M. & Goslin, J. Interaction between the Mid-Atlantic Ridge and the Azores hot spot
301 during the last 85 Myr: Emplacement and rifting of the hot spot-derived plateaus. *Geochemistry*
302 *Geophys. Geosystems* **4**, 1–23 (2003).
- 303 37. Pinto Ribeiro, L., Martins, S., Hildenbrand, A., Madureira, P. & Mata, J. The genetic link between the
304 Azores Archipelago and the Southern Azores Seamount Chain (SASC): The elemental , isotopic and
305 chronological evidences. *Lithos* **295**, 133–146 (2017).
- 306 38. Duncan, R. A. Hotspots in the southern oceans - an absolute frame of reference for motion of the
307 gondwana continents. *Tectonophysics* **74**, 29–42 (1981).

- 308 39. Müller, R. D., Royer, J.-Y. & Lawver, L. A. Revised plate motions relative to the hotspots from
309 combined Atlantic and Indian Ocean hotspot tracks. *Geology* **21**, 275–278 (1993).
- 310 40. Whittaker, J. M. *et al.* Long-term interaction between mid-ocean ridges and mantle plumes. *Nat. Geosci.*
311 **8**, 1–6 (2015).
- 312 41. Molnar, P. & Stock, J. Relative motions of hotspots in the Pacific, Atlantic and Indian Oceans since late
313 Cretaceous time. *Nature* **327**, 587–591 (1987).
- 314 42. Hassan, R., Müller, R. D., Gurnis, M., Williams, S. E. & Flament, N. A rapid burst in hotspot motion
315 through the interaction of tectonics and deep mantle flow. *Nature* **533**, 239–242 (2016).
- 316 43. Steinberger, B. & O’Connell, R. J. Advection of plumes in mantle flow : implications for hotspot
317 motion, mantle viscosity and plume distribution. *Geophys. J. Int.* **132**, 412–434 (1998).
- 318 44. Thorne, M. S. & Garnero, E. J. Inferences on ultralow-velocity zone structure from a global analysis of
319 SPdKS waves. *J. Geophys. Res.* **109**, 1–22 (2004).
- 320 45. McNamara, A. K. & Zhong, S. The influence of thermochemical convection on the fixity of mantle
321 plumes. *Earth Planet. Sci. Lett.* **222**, 485–500 (2004).
- 322 46. Flament, N., Williams, S., Müller, R. D., Gurnis, M. & Bower, D. J. Origin and evolution of the deep
323 thermochemical. *Nat. Commun.* (2017). doi:10.1038/ncomms14164
- 324 47. Ni, S., Tan, E., Gurnis, M. & Helmberger, D. Sharp Sides to the African Superplume. *Science (80-.).*
325 **296**, (2002).
- 326 48. Herzberg, C. & Asimow, P. D. Petrology of some oceanic island basalts: PRIMELT2.XLS software for
327 primary magma calculation. *Geochemistry Geophys. Geosystems* **9**, (2008).
- 328 49. Tackley, P. J. Modelling compressible mantle convection with large viscosity contrasts in a three-
329 dimensional spherical shell using the yin-yang grid. *Phys. Earth Planet. Inter.* **171**, 7–18 (2008).
- 330 50. Coltice, N. & Shephard, G. E. Tectonic predictions with mantle convection models. *Geophys. J. Int.*
331 (2018). doi:10.1093/gji/ggx531
- 332 51. Ricard, Y. A geodynamic model of mantle density heterogeneity. *J. Geophys. Res.* **98**, 895–909 (1993).
- 333 52. Nakiboglu, S. M. & Lambeck, K. Deglaciation effects on the rotation of the Earth. *Geophys. J. R. Astr.*
334 *Soc.* **62**, 49–58 (1980).
- 335 53. Tackley, P. J. Self-consistent generation of tectonic plates in three-dimensional mantle convection. *Earth*
336 *Planet. Sci. Lett.* **157**, 9–22 (1998).
- 337 54. Debayle, E., Dubuffet, F. & Durand, S. An automatically updated S -wave model of the upper mantle
338 and the depth extent of azimuthal anisotropy. *Geophys. Res. Lett.* (2016). doi:10.1002/2015GL067329.1.
- 339 55. Herzberg, C. & Asimow, P. D. PRIMELT3 MEGA.XLSM software for primary magma calculation:
340 Peridotite primary magma MgO contents from the liquidus to the solidus. *Geochemistry Geophys.*
341 *Geosystems* **16**, 563–578 (2015).
- 342

343 **SUPPLEMENTARY INFORMATION**

344 **Supplementary Information** is linked to the online version of the paper at www.nature.com/nature

345

346

347 **ACKNOWLEDGEMENTS**

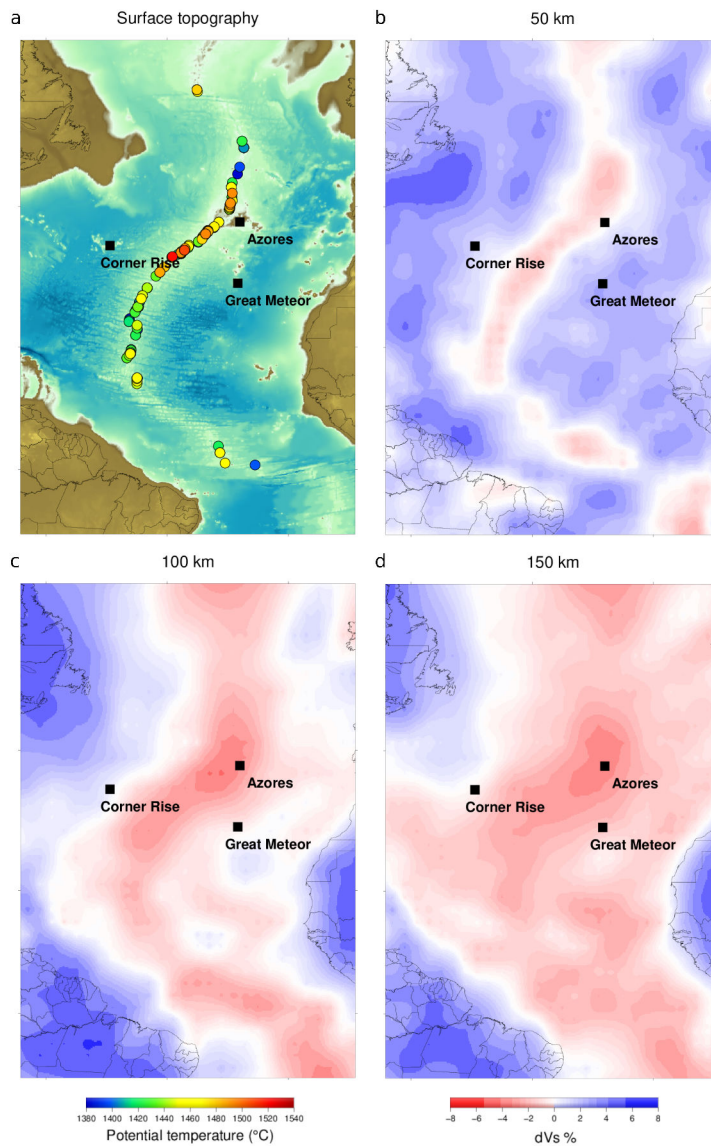
348 The research leading to these results has received funding from the IRD, CNRS-INSU and the European
349 Research Council within the framework of the SP2-Ideas Program ERC-2013-CoG, under ERC grant agreement
350 617588. Calculations were performed with the assistance of resources from the National Computational
351 Infrastructure (NCI) through the National Computational Merit Allocation Scheme supported by the Australian
352 Government.

353

354 **AUTHOR CONTRIBUTIONS**

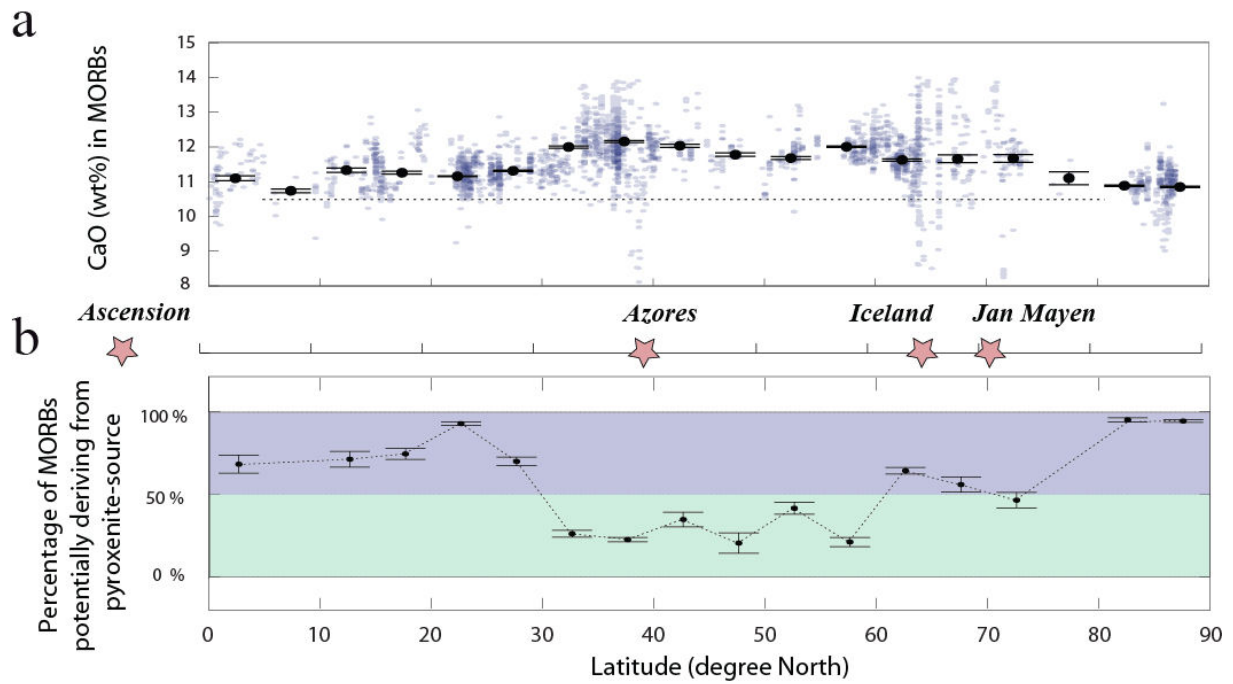
355 M.A. and J.G. conceived the study and wrote the paper. N.C. helped to generate the research idea and
356 contributed to the writing and focusing of the paper. J.G. contributed with X.F. to the petrologic analysis and
357 PRIMELT modelling. M.A and N.C. developed the numerical models and the kinematic analysis of the Azores
358 plume motion. All authors contributed to the interpretation of results.

359



360
 361
 362
 363
 364
 365

Figure 1– (a) Surface topography of the Central Atlantic Ocean and potential temperatures obtained from the PRIMELT method along the MAR (see **Fig. 3**). (b-d) Upper mantle shear wave tomography slices from the global upper mantle and transition zone model 3D2017_09SV⁵⁴.



366

367

368 **Figure 2** - (a) Chemical evolution of (near zero-age) MORBs sampled along the Mid-Atlantic Ridge. Data have

369 been plotted against the latitudes between 0 and 90°N along the x-axis. The Jan Mayen, Iceland and Azores

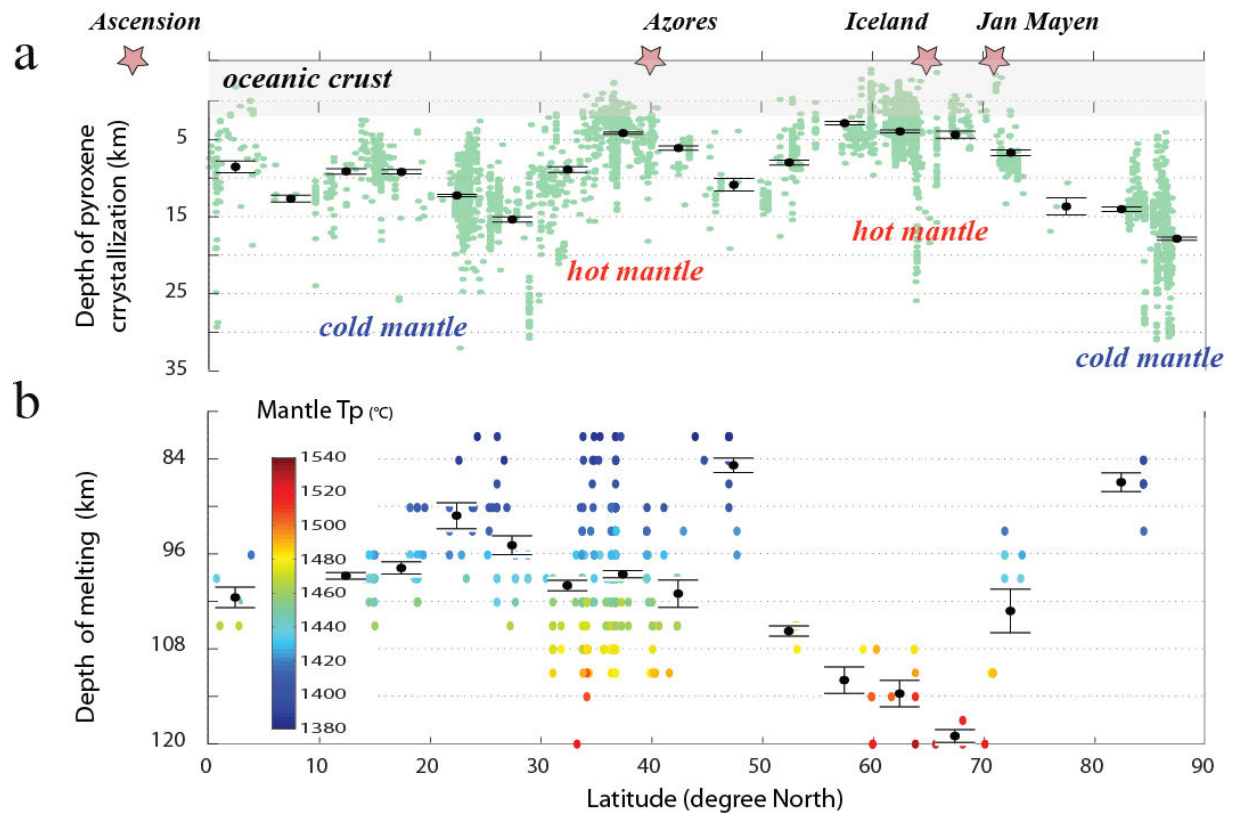
370 plume-like volcanic edifices forming on the ridges are indicated. (b) Percentage of MORBs for which PRIMELT

371 predicts a primary magma composition depleted in calcium. Mean values (black points), obtained by bootstrap

372 analysis, are reported at 5° step of latitude.

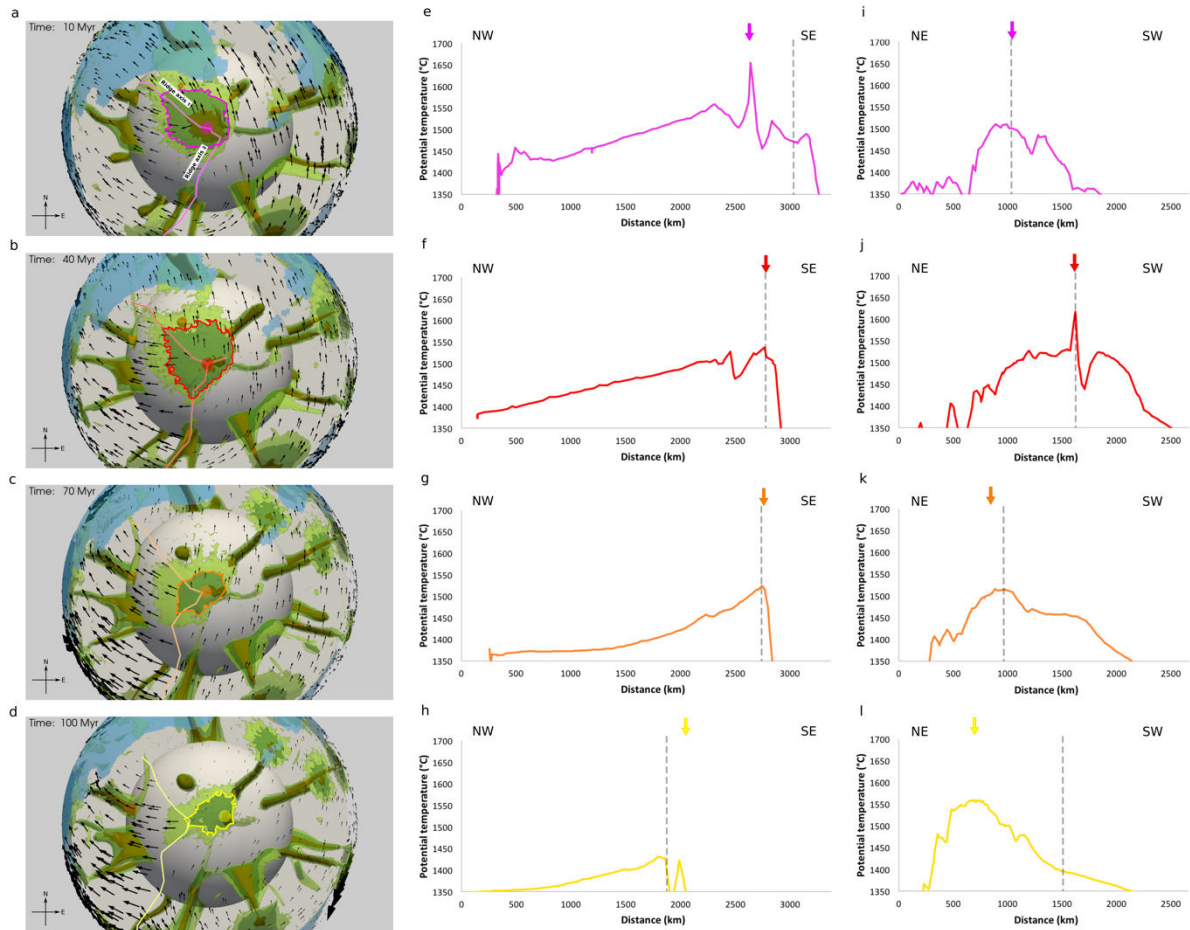
373

374



375

376 **Figure 3** – (a) Depth of pyroxene crystallization then subtraction (e.g. fractionation) in a primary magma that,
 377 later, will give birth to MORBs, calculated using equation (6) in Herzberg, 2004²⁵ and assuming a ratio of 1:3
 378 between pressure (kb) and depth (km). Data have been plotted against latitudes along the x-axis. (b) Depth at
 379 which adiabatically upwelling mantle below the MAR segments crossed their solidus, depending on their
 380 potential temperature (T_p) calculated with PRIMELT3 MEGA software⁵⁵ using reduced conditions ($Fe^{2+}/\Sigma Fe =$
 381 0.9) in the source. Solutions of calculation have been filtered for $MgO < 8$ wt% (blue dots in **Fig. 2 SI**). Mean
 382 values (black points), obtained by bootstrap analysis, are reported at 5° step of latitude.



383

384

385

386

387

388

389

390

391

392

393

394

Figure 4 – (a-d) Temporal evolution of the relative position of a ridge (straight colored lines) and a mantle plume in a global mantle convection model self-generating plate-like tectonics. Colored contour lines outline the studied mantle plume isotherm 1480°C at (a) 10 My (magenta), (b) 40 My (red), (c) 70 My (orange) and (d) 100 My (yellow). The transparent filled circles show the location of the plume head maximum of temperature near the surface. Brown, dark green and light green contours show the location of mantle plume through depth by delimitating the 1700°C (0.9), 1480°C (0.8) and 1390°C (0.76) isotherms, respectively. Black arrows scale with surface plate velocities and blue transparent areas show the location of continents. (e-h) Temporal evolution of the potential temperature distribution at 110 km depth along ridge axis 1 and (i-l) ridge axis 2 (see (a) for location) at 10 My (magenta), 40 My (red), 70 My (orange) and 100 My (yellow). The colored arrows correspond to the location of the plume maximum of temperature at corresponding time steps. The grey dashed lines show the junction between ridge axis 1 and 2.